Arabian Journal of Geosciences (2021) 14:1232
https://doi.org/10.1007/s12517-021-07593-3

S. I. SCJGE-1 2019

Geochemical insight into granite hosted U-rich fluorite, Gabal El-Erediya area, Central Eastern Desert, Egypt: REE geochemical and fluid inclusion aspects

Omar Amer[1] · Sherif Kharbish[2] · Ali Maged[2] · Fares Khedr[2]

Received: 30 March 2021 / Accepted: 10 June 2021
© Saudi Society for Geosciences 2021

Abstract

The A-type younger granite pluton and associated fluorite of Gabal El-Erediya, Eastern Desert, Egypt, have been investigated geologically and geochemically. Granites are genetically high-K-calc-alkaline syenogranites that show a high LREE/HREE ratio with noticeable negative Eu anomaly. Additionally, the visible tetrad pattern and negative Eu anomaly of the investigated granites point to fractional crystallization and fluid-melt interactions during the last stage of magmatic differentiation. They were probably generated within an extensional environment and were crystallized at temperature ~ 740 °C and pressure ~ 1.9 kbars. Two types of U-rich fluorite mineralizations were recorded including colorless and violet types. The hydrothermal fluids forming fluorites were related to late-stage differentiation of the felsic magma with a crystallization temperature ranging from 118 to 336 °C.

Keywords Granite · Fluorite · Uranium · Felsic · Hydrothermal

Introduction

El-Erediya younger granitoids (ErdYG) belong to the basement rocks group located in the Egyptian Eastern Desert (EED) (Fritz et al. 2013), which represents a NW segment of the Arabian-Nubian Shield (ANS). In the last decennium, several significant studies were reported and focused on the geological features and tectonics of Egyptian ANS (Kharbish 2010, 2020; Kharbish and Elawadi 2018; Elwan et al. 2019; Kharbish and El-Awady 2019). The Egyptian younger granites (EYG) (550–610 Ma, (Beyth et al. 1994)), that developed during extension, composed mainly of syeno-, monzo-, and alkali-feldspar granites.

This article is part of the Topical Collection on *Current Advances in Geological Research of Egypt*

Omar Amer and Sherif Kharbish share co-first authorship.

Responsible Editor: Zakaria Hamimi

✉ Ali Maged
Ali.Maged@Suezuni.edu.eg

[1] Geology Department, Faculty of Science, Zagazig University, City, Sharkia Governorate, Zagazig 44519, Egypt

[2] Geology Department, Faculty of Science, Suez University, El Salam City Governorate, P.O. Box 43518, Suez, Egypt

Fluorite, which forms in various geological environments, may be considered as a geochemical and field guide for U deposits. It plays an important role in the transportation of many rare elements in different magmas which give a special significance to the studies of their behavior, contents, and distribution of fluorine in granitic rocks (Kovalenko 1971). A direct relation between the contents of beryllium, tantalum, tin, and fluorine in the granitoid rocks exists, which is accordingly considered as a criterion of mineralization in geochemical prospecting for these metals (Odikadze 1971). Additionally, fluorite is believed to precipitate during magmatic and/or magmatic-hydrothermal stages (Nash 1993; Webster and Duffield 1994).

The U-rich igneous rocks are considered as a significant source of metals in U mineral systems. The relationship is manifested by the wide spatial correlation between known U deposits and igneous rocks containing high abundances of U (Lambert et al. 2005). Generally, U is initially mobilized from igneous rocks by hydrothermal and/or surficial fluids (Cuney 2014; Saleh and Kamar 2018), whereas U deposits resulting only from the magmatic process (partial melting or fractional crystallization) are rare (IAEA 2012).

The common U sources in Egypt are mainly classified into (1) metasomatized granites as represented in Gabal Um Ara

Published online: 22 June 2021

(Saleh and Kamar 2018); (2) vein-type mineralization as found in El-Sela area (Ghoneim and Gawad 2018); (3) two-mica granites as represented in Gabal Ribdab area (Ibrahim et al. 2001); (4) sheared zones calc-alkaline granite as represented in Gabal Gattar (Mahdy et al. 2014); and (5) lamprophyre dikes bearing-REEs and U as found in Abu Rusheid area (Ibrahim et al. 2015).

The U-F geochemical integrations in igneous rocks suggested that U transported as complex fluoride compounds and the source for U is a highly advanced F granitic magma. Practically, the U-F mineralizations localized in all volcanic, sedimentary, as well as granitic and metamorphic rocks (Aleshin et al. 2002, 2007; Kharbish et al. 2021). In the granite-hosted U deposits, the potentiality of U mineralization is controlled by many factors including the physical and chemical conditions, the abundance of F (has a great effect in decreasing the crystallization temperature), the oxidation degree, and the concentration of U in granitic magma (Zhao et al. 2011; Chen et al. 2012).

The central EED is considered as one of the most important U-F occurrences in Egypt. The ErdYG in the central EED have been found hosting significant uranium-fluorite (U-F) mineralization (Ibrahim et al. 2004). The present article designed to get insight into the geochemical characteristics and geotectonic consequences of A-type granites pluton (El-Erediya) detected in the central EED. Moreover, this work focuses on the mode of occurrence and genesis of the related fluorite deposits using the present geochemical data and fluid inclusions in fluorite. Besides, explore the relation between fluorites and the hosted granitic pluton.

Geological setting and petrography

Gabal El-Erediya is an oval-shaped outline and elongated granite intrusion. It covers nearly 16 km^2 between latitudes 26° 15′–26° 25′ N and longitudes 33° 22′–33° 30′ E **(Fig. 1)**. This locality also comprises several rock units that represent from oldest to youngest: metavolcanics, older granites, younger gabbros, and younger granites (Moussa 2006) **(**Fig. 1**)**. The ErdYG is dissected by two main faulting trends (NW-SE and N-S), which play an important role in pathways for different hydrothermal or meteoric solutions, which cause different types of hydrothermal alterations (i.e., hematitization, kaolinitization, sericitization, and fluoritization).

El-ErdYG are medium-grained in size, color range from pink to red, and present pan idiomorphic and porphyritic textures. ErdYG are constituted mostly of quartz, plagioclases, and K-feldspars (microcline and microcline perthites). Furthermore, biotites, fluorite, monazite, allanite, muscovites, zircon, apatite, and opaques are also found in the ErdYG in small quantities as accessory minerals (Moussa 2006). U-fluorite mineralization is essentially associated with fluoritized-hematitized sheared-granite zones, mainly along NW-SE and N-E faults **(**Fig. 1**)**. U-fluorite crystals occur as small irregular grains filling cracks and cavities in the host rocks. They vary in color from colorless to dark violet, and their size correlates positively with the degree of alterations.

Sampling and experimental setup

Nineteen samples were investigated in detail [eight samples from granites **(**Table 1**)** and eleven U-rich fluorites **(**Table 2**)**]. X-ray fluorescence (XRF) technique was applied to define both major and trace element concentrations using fused and pressed powder disks, respectively. XRF analyses (Philips PW 2400 series spectrometer) were carried out at Vienna University, Austria (the Earth Science Institute). In order to determine the loss on ignition (LOI), a precise weight (5 g) amount of each powdered sample was igniting in porcelain crucibles for 1 h at 1050 °C. For major and trace elements, analytical accuracy was greater than 1% and 2–5%, respectively. International standards such as African Mineral Standards (AMIS 0007) have been employed to verify the analytical accuracy and precision for the analyzed blanks, samples, and duplicates. REE concentrations were measured at Vienna University, Austria (the Institute of Inorganic Chemistry), using the coupled plasma-mass spectrometer (VG Elemental PQ3 Quadrupole Inductively). Ten fluorite samples were used to prepare the doubly polished fluid inclusion sections (100–150-μm thick). The microthermometric analyses were conducted on four selected sections that are characterized by a dense population of fluid inclusions. The inclusions were subjected to freezing measurements first to avoid stretching and false homogenization temperatures. Linkam THM 600 heating-freezing stage was utilized for the determinations of homogenization temperature (T_h) and melting temperature (T_m). The stage was installed on a microscope (Olympus BX 60) and calibrated by employing artificial fluid inclusions at − 56.6 (melting of pure CO_2), 0.0 (melting of pure H_2O), and 374.0 °C (critical homogenization of pure H_2O). The temperature measurement precision was found to be 0.1 °C for the ending melting temperatures (T_m). However, the temperatures were found in ranges from – 100 °C to + 250 °C for the homogenization temperatures (T_h). The inclusion investigations were conducted at Vienna University, Austria (the Institute of Mineralogy and Crystallography).

Results and discussion

Whole-rock major and trace element geochemistry

ErdYG are described by limited high ranges of SiO_2 (74.93–75.52 Wt.%) and a high range (8.09–8.23 Wt. %) of the alkali

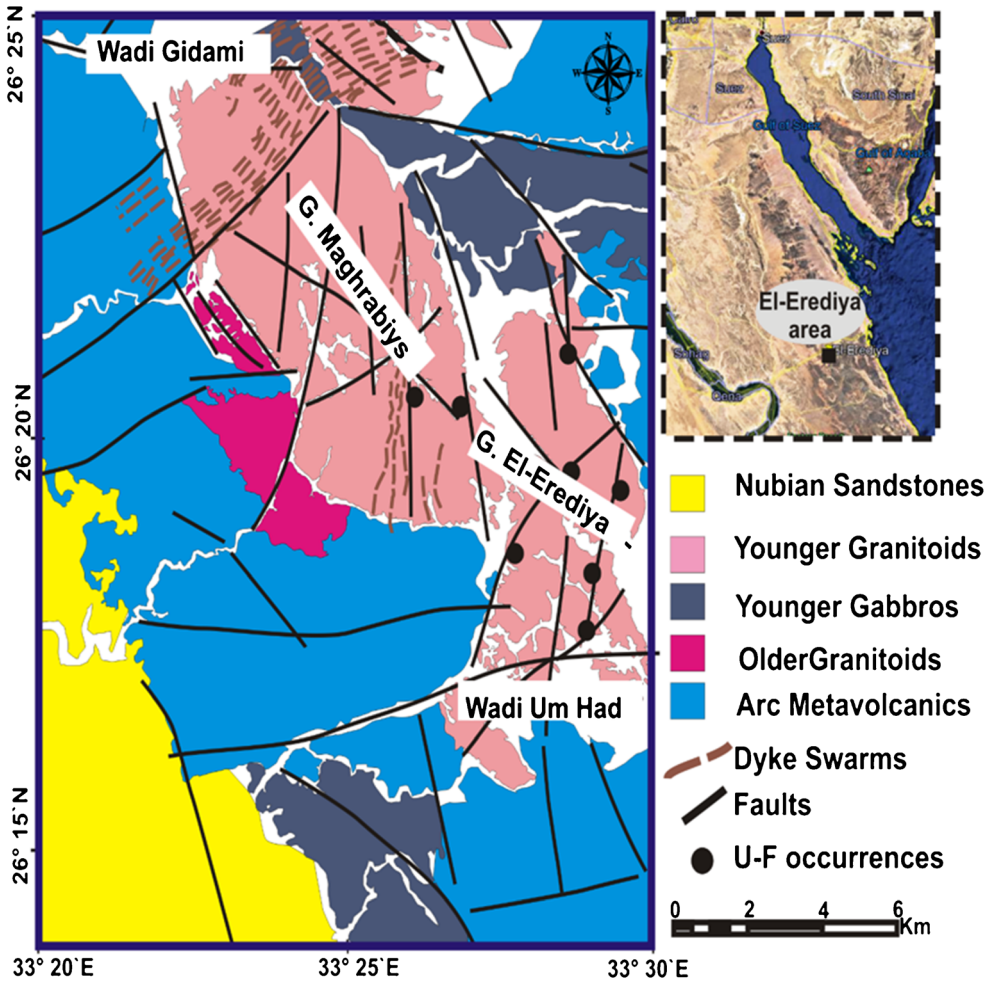

Fig. 1 Geological map of El-Erediya area, Central Eastern Desert, Egypt (modified after Bakhit and El Kassas 1989; Abu Dief 1993)

(Na_2O+K_2O) contents. Besides, the K_2O/Na_2O ratios were found to be in the ranges from 1.05 to 1.10 (Table 1); these values could probably be due to K-feldspar accumulation. ErdYG are also characterized by the presence of high alkali metal contents in addition to the high field strength elements (HFSE). However, ErdYG were found of low contents for Ba (49.08 ppm), Sr (17.73 ppm), Hf (9.69 ppm), and Eu (0.32 ppm) (Table 1). ErdYG are slightly peraluminous (Fig. 2A, aluminum saturation index (ASI) varies from 1.01 to 1.02), strongly differentiated (Fig. 2B) syenogranites (Fig. 2C). ErdYG are highly fractionated calc-alkaline (HFCA) rocks (Fig. 2D), belonging to the Egyptian calc-alkaline younger granites field (Fig. 2E), and represented in the series which have a high value of K-calc-alkaline and shoshonite (Fig. 2F). The studied samples were found in the mineralized field (Fig. 2G) according to Tischendorf (1977).

The K/Rb ratios are considered a good indicator in determining the state of transition of granite melts; when the K/Rb ratios are lower than 100 (K/Rb = 38.99–39.74 in the analyzed samples), the granites are characterized to be highly evolved (Rossi et al. 2011). These observations occur because Rb tends to concentrate relative to K in the strongly differentiated granitic melt during the segregation stage of aqueous liquid phases from the remaining silicate melts (Elwan et al. 2019) or in the granite that was subjected to late and post-magmatic alterations (Tischendorf 1977). Furthermore, the binary diagram of SiO_2-K/Rb also supports the strongly evolved and fractionated nature of the granitic melt (Fig. 2H) for the ErdYG (Blevin 2003).

Figure 2K shows the REE chondrite-normalized patterns of the ErdYG. The obtained results demonstrate flat patterns along with strong negatively Eu anomalies with a ratio (Eu/Eu*) range from 0.1 to 0.16 and "tetrad effect" (Bau 1996). REE chondrite-normalized patterns also characterized by insignificant fractionations LREE (which represent by $(La/Sm)_N$= 1.01–1.72) as well as HREE ($(Gd/Yb)_N$= 0.92–4.77). However, the REE chondrite-normalized pattern displays slightly enhanced LREE values compared to HREE, ($(La/Yb)_N$ = 1.05–5.33) and nearly flat heavy REE [HREE, $(Ho/Lu)_N$ = 0.46–1.76]. The REEs normalized patterns of El-Erediya syenogranite (ErdSG) are consistent with those of Sinai calc-alkaline granitoids (Eyal et al. 2010) with slightly enriched HREEs for the Sinai granitoids (Fig. 2K). ErdSG displays strong negative anomalies (Fig. 2M) for P, Ba, Sr,

Table 1 Major oxides (wt %); trace, rare earth elements (ppm) and some geochemical ratios for the studied El-Erediya granites

Sample	GR1	GR2	GR3	GR4	GR5	GR6	GR7	GR8	Avg.
Major oxides (wt %)									
SiO_2	75.01	74.93	75.52	75.49	75.04	75.14	75.16	75.26	75.19
Al_2O_3	12.67	12.81	12.87	12.77	12.77	12.75	12.81	12.77	12.78
Fe_2O_3	1.64	1.72	1.48	1.36	1.76	1.57	1.65	1.56	1.59
MgO	0.02	0.02	0.03	0.02	0.02	0.02	0.02	0.02	0.02
CaO	0.83	0.85	0.89	0.88	0.83	0.85	0.85	0.86	0.86
Na_2O	3.91	3.96	3.95	3.94	3.92	3.93	3.94	3.93	3.94
K_2O	4.18	4.22	4.28	4.15	4.31	4.18	4.27	4.23	4.23
TiO_2	0.05	0.05	0.06	0.06	0.05	0.05	0.05	0.05	0.05
P_2O_5	0.01	0.01	0.01	0.01	0.01	0.01	0.01	0.01	0.01
MnO	0.04	0.04	0.05	0.05	0.04	0.04	0.04	0.04	0.04
F	0.16	0.17	0.13	0.12	0.18	0.15	0.16	0.15	0.15
LOI	0.76	0.71	0.8	0.86	0.7	0.77	0.74	0.78	0.77
Total	99.28	99.49	100.07	99.71	99.63	99.46	99.7	99.66	99.63
CIPW norms									
Quartz	34.45	33.88	34.21	34.78	33.92	34.42	34.04	34.33	34.25
Orthoclase	24.7	24.94	25.29	24.52	25.47	24.7	25.23	25	24.98
Albite	33.08	33.51	33.42	33.34	33.17	33.25	33.34	33.25	33.3
Anorthite	4.07	4.17	4.37	4.32	4.07	4.17	4.17	4.22	4.19
Zircon	0.12	0.12	0.06	0.06	0.12	0.1	0.1	0.09	0.09
Ilmenite	0.08	0.09	0.11	0.11	0.09	0.09	0.08	0.09	0.09
Corundum	0.22	0.2	0.14	0.21	0.17	0.23	0.18	0.18	0.19
Magnetite	0.02	0	0	0	0	0	0.02	0	0
Hematite	1.63	1.72	1.48	1.36	1.76	1.57	1.64	1.56	1.59
Hypersthene	0.05	0.05	0.07	0.05	0.05	0.05	0.05	0.05	0.05
Apatite	0.02	0.02	0.02	0.02	0.02	0.02	0.02	0.02	0.02
Trace elements (ppm)									
Ba	44.5	46.5	55	51	48.5	47.3	50	49.8	49.08
Be	17.5	16	17.5	18.5	16.5	17.3	16.7	17.5	17.19
Co	2.2	2.1	2.1	2.2	2.1	2.1	2.1	2.1	2.13
Cs	10.1	10	10.1	10	10.1	10	10	10.1	10.05
Ga	32	29.5	33.5	32.5	33	31.3	32	32.8	32.08
Hf	9.8	9.4	9.8	9.7	9.8	9.6	9.6	9.8	9.69
Nb	75.2	74	61.2	68	68.4	72.4	67.8	68.2	69.4
Rb	888.2	895.7	894.2	883.7	898.7	889.2	896.2	891.2	892.14
Sn	27.5	28.5	27.5	26	29	27.3	28.3	27.5	27.7
Sr	19	17.5	16.6	17.7	17.9	18	17.3	17.8	17.73
Ta	10.7	9.9	9.6	10.5	9.8	10.4	9.8	10.2	10.11
V	8	7.5	7.5	7.5	8	7.7	7.7	7.8	7.71
W	25.3	26.2	23.8	24.3	24.8	25.3	24.9	24.6	24.9
Zr	574.5	576	316	299	591.5	483.2	494.5	445.3	472.5
Y	148.5	148	140	141.5	147	146	145	144.3	145.04
Mo	22	22.1	21.7	21.6	22.1	21.9	21.9	21.8	21.89
Cu	3.2	3.3	3.1	3.1	3.2	3.2	3.2	3.1	3.18
Pb	20.3	21.9	20.4	20	20.7	20.7	21	20.3	20.66
Zn	159	155	148.5	157	150.5	157	151.3	153.8	154.01
Ni	4.8	4.9	4.8	4.8	4.9	4.8	4.8	4.8	4.83
As	0.8	0.9	0.9	0.8	0.8	0.8	0.8	0.8	0.825
Cd	0.1	0.1	0.1	0.1	0.1	0.1	0.1	0.1	0.1

Table 1 (continued)

Sample	GR1	GR2	GR3	GR4	GR5	GR6	GR7	GR8	Avg.
Sb	0.2	0.2	0.2	0.2	0.2	0.2	0.2	0.2	0.2
Bi	0.9	0.9	0.9	0.9	0.9	0.9	0.9	0.9	0.9
Ag	0.3	0.3	0.3	0.3	0.3	0.3	0.3	0.3	0.3
U	29.4	31.9	29.2	25.5	33	28.9	31.3	29.3	29.81
Th	34.3	36.3	31.5	30.5	35.3	33.7	34.3	32.9	33.6
REEs (ppm)									
La	16.02	14.73	14.25	13.22	16.04	14.62	15.38	14.66	14.87
Ce	36.82	36.45	41.05	40.09	38.21	38.45	37.33	38.25	38.33
Pr	3.58	4.21	5.12	3.84	4.11	3.71	4.16	4.05	4.1
Nd	20.71	18.24	19.42	11.05	17.35	15.88	17.81	15.57	17
Sm	5.11	8.02	7.22	6.78	7.84	5.94	7.93	7.54	7.05
Eu	0.37	0.29	0.41	0.28	0.29	0.35	0.29	0.28	0.32
Gd	10.15	8.74	9.42	8.55	11.24	9.35	9.99	9.51	9.62
∑LREEs	92.76	90.68	96.89	83.81	95.08	88.3	92.89	89.86	91.28
Tb	1.72	0.98	1.53	2.07	1.44	1.9	1.21	1.49	1.54
Dy	10.25	11.71	9.08	8.73	12.14	9.49	11.93	10.86	10.52
Ho	3.08	1.78	4.11	2.49	2.41	2.79	2.09	2.23	2.62
Er	8.41	7.11	6.89	7.21	6.45	7.81	6.78	6.92	7.2
Tm	1.28	1.73	2.04	0.98	1.16	1.13	1.44	1.29	1.38
Yb	6.72	5.04	8.24	1.45	5.49	4.09	5.27	3.99	5.04
Lu	0.99	1.17	1.05	2.45	1.13	1.72	1.15	1.58	1.405
∑HREEs	32.45	29.52	32.94	25.38	30.22	28.93	29.87	28.36	29.71
Some geochemical ratios									
Zr/Hf	58.62	61.28	32.24	30.82	60.36	50.33	51.51	45.44	48.77
Nb/Ta	7.03	7.47	6.38	6.48	6.98	6.96	6.92	6.69	6.86
Rb/Sr	46.75	51.18	53.87	49.93	50.21	49.4	51.8	50.07	50.40
(Tb/Yb)N	1.09	0.83	0.79	6.07	1.12	1.98	0.98	1.59	1.3
(La/Yb)N	1.44	1.77	1.05	5.53	1.77	2.17	1.77	2.23	1.79
(La/Sm)N	1.72	1.01	1.08	1.07	1.12	1.35	1.06	1.07	1.16
(Gd/Yb)N	1.22	1.40	0.92	4.77	1.66	1.85	1.53	1.93	1.55
Eu/Eu*	0.16	0.11	0.15	0.11	0.1	0.14	0.1	0.1	0.12
(Ho/Lu)N	1.40	0.69	1.76	0.46	0.96	0.73	0.82	0.64	0.84
(La/Lu)N	1.68	1.31	1.41	0.56	1.47	0.88	1.39	0.96	1.10
Ce/Ce*	1.18	1.12	1.16	1.36	1.14	1.26	1.13	1.20	1.19
K_2O/ Na_2O	1.07	1.07	1.08	1.05	1.10	1.06	1.08	1.08	1.07
ASI	1.02	1.01	1.01	1.02	1.01	1.02	1.01	1.01	1.01
K/Rb	39.07	39.11	39.74	38.99	39.81	39.03	39.56	39.4	39.34
T_Al/Ti.exp.C	717.3	738.5	756.7	757.5	738.8	739	716.3	738.8	737.86
P kbar	1.80	1.95	1.86	1.71	1.94	1.81	1.91	1.83	1.85
Depth	6.4	7	6.7	6.1	6.9	6.5	6.8	6.6	6.6
Log fO_2	− 15.81	− 15.28	− 14.84	− 14.82	− 15.27	− 15.26	− 15.83	− 15.27	− 15.30
TE_{1-3}	0.87	1.02	0.91	1.23	0.98	1.02	1	1.07	1.01
Ca/Sr	312.21	347.14	383.18	355.33	331.4	337.5	351.15	345.3	344.75
Rb/Ba	19.96	19.96	19.96	19.96	19.96	19.96	19.96	19.96	19.96
K/Ba	779.83	753.43	646.05	675.55	737.77	733.67	708.99	705.17	715.16

Table 2 Chemical analyses of the El-Erediya fluorites

	Violet fluorite						Colorless fluorite						
	F1	F2	F3	F4	F5	Avg.	F6	F7	F8	F9	F10	F11	Avg.
Element %													
Si	0.07	0.05	0.06	0.07	0.07	0.06	0.10	0.05	0.04	0.05	0.09	0.08	0.07
Al	0.07	0.06	0.04	0.07	0.05	0.06	0.08	0.07	0.06	0.05	0.03	0.08	0.06
Ti	0.02	0.01	0.02	0.01	0.02	0.02	0.03	0.02	0.01	0.01	0.03	0.01	0.02
Ca	55.82	55.13	54.97	55.06	55.12	55.22	55.42	55.38	56.21	54.87	53.73	55.24	55.14
Na	0.04	0.03	0.06	0.05	0.04	0.04	0.02	0.01	0.05	0.04	0.07	0.06	0.04
Mn	0.02	0.02	0.02	0.01	0.01	0.02	0.01	0.02	0.02	0.01	0.01	0.02	0.02
Fe	0.05	0.03	0.05	0.04	0.04	0.04	0.01	0.05	0.09	0.01	0.01	0.07	0.04
P	0.11	0.11	0.09	0.04	0.09	0.09	0.09	0.17	0.12	0.05	0.07	0.03	0.09
F	42.92	44.13	42.88	44.03	43.03	43.40	43.25	43.89	42.58	44.36	43.18	43.69	43.49
total	99.12	99.57	98.19	99.37	98.47	98.94	99.01	99.66	99.18	99.45	97.22	99.28	98.97
Ti	431.60	425.90	515.50	428.80	470.70	454.5	1142.1	1087.2	1232.7	1024.7	1197.48	1074.4	1126
Trace ppm													
Ba	45.00	45.00	45.80	45.00	45.40	45.24	731.02	694.25	789.54	421.31	609.78	713.25	659.9
Co	0.80	0.90	0.80	0.80	0.90	0.84	3.87	4.12	4.36	3.85	2.08	6.78	4.18
Cr	7.60	8.50	6.40	8.00	7.40	7.58	6.40	4.80	4.60	4.70	9.80	9.50	6.63
Cu	18.00	18.00	17.50	18.00	17.80	17.86	14.50	14.40	13.20	15.70	13.80	14.50	14.35
Li	0.90	0.20	0.40	0.50	0.30	0.46	0.70	0.70	0.70	0.70	0.70	0.70	0.70
Mo	43.50	8.00	23.80	25.80	15.90	23.40	0.45	0.42	0.44	21.62	21.74	21.68	11.06
Ni	9.00	11.40	11.30	10.20	11.40	10.66	11.47	10.30	10.70	11.40	10.50	11.10	10.91
Pb	631.00	635.00	641.50	633.00	638.3	635.7	643.80	649.50	646.65	54.80	55.00	54.90	350.8
Rb	18.70	19.00	18.50	18.90	18.8	18.78	147.25	132.45	173.26	98.83	166.42	158.25	146.1
Sr	58.40	58.60	58.60	58.50	58.60	58.54	265.71	280.28	371.25	274.62	311.05	299.78	300.5
Zn	476.50	486.00	483.50	481.30	484.8	482.4	635.00	614.00	674.00	624.50	644.00	541.23	622.1
Sb	0.10	0.10	0.10	0.10	0.10	0.10	0.10	0.10	0.10	0.10	0.10	0.10	0.10
V	0.80	0.80	0.80	0.80	0.80	0.80	35.75	42.15	39.58	27.20	44.99	37.81	37.91
Zr	83.50	87.60	112.30	85.60	99.90	93.78	111.24	108.35	123.12	127.23	134.23	155.47	126.6
Rare ppm													
La	54.40	54.40	50.20	54.40	52.30	53.14	12.47	7.59	11.24	1.89	0.77	8.45	7.07
Ce	181.00	181.00	179.80	181.00	180.4	180.6	16.35	20.21	16.87	35.01	40.71	27.52	26.11
Pr	23.40	23.40	22.70	23.40	23.10	23.20	2.81	1.78	0.73	0.26	0.10	1.89	1.26
Nd	98.30	98.30	100.30	98.30	99.30	98.90	8.43	11.49	15.82	1.92	0.99	5.09	7.29
Sm	26.40	26.40	27.90	26.40	27.20	26.86	3.58	2.74	0.89	0.74	1.99	3.05	2.17
Eu	0.40	0.60	0.50	0.50	0.60	0.52	0.42	0.47	0.51	0.39	0.44	0.42	0.44
Gd	33.90	33.80	34.60	33.80	34.20	34.06	3.19	4.21	5.39	1.94	2.96	3.42	3.52
∑LREEs	417.80	417.90	416.00	417.80	417.1	417.3	47.25	48.49	51.45	42.15	47.96	49.84	47.86
Tb	6.10	6.10	5.60	6.10	5.90	5.96	0.91	0.57	0.68	0.82	0.28	0.51	0.63
Dy	47.80	47.30	46.90	47.60	47.10	47.34	5.79	2.69	3.45	4.71	5.09	2.98	4.12
Ho	14.30	14.30	13.90	14.30	14.10	14.18	0.34	0.56	1.78	1.22	0.38	0.49	0.80
Er	53.10	55.90	54.80	54.50	55.30	54.72	1.49	2.85	3.41	4.61	3.73	1.44	2.92
Tm	8.70	8.70	8.90	8.70	8.80	8.76	0.42	0.29	0.83	0.34	0.41	0.74	0.51
Yb	80.60	72.80	77.20	76.70	75.00	76.46	6.41	2.87	2.95	4.91	3.71	2.99	3.97
Lu	13.60	13.60	13.80	13.60	13.70	13.66	0.28	0.31	0.26	0.33	0.35	0.42	0.33
∑HREEs	224.20	218.70	221.10	221.50	219.9	221.1	15.64	10.14	13.36	16.94	13.95	9.57	13.27
∑REE	642.00	636.60	637.10	639.30	637	638.4	62.89	58.63	64.81	59.09	61.91	59.41	61.13
Y	1061	1068	1060.8	1064.5	1064.4	1064	147.62	83.78	76.72	19.85	45.78	104.22	79.66
Sc	95.00	0.00	47.50	47.50	23.80	42.76	9.55	10.06	11.02	9.74	7.59	9.42	9.56

Table 2 (continued)

	Violet fluorite						Colorless fluorite						
	F1	F2	F3	F4	F5	Avg.	F6	F7	F8	F9	F10	F11	Avg.
Th	259.00	241.50	267.80	250.30	254.6	254.6	27.58	77.45	65.89	7.89	71.73	64.95	52.58
U	490.10	496.20	491.50	493.10	493.8	492.9	142.23	134.96	85.44	62.08	117.83	138.73	113.6
Nb	8.61	7.97	9.58	8.30	8.07	8.51	7.45	3.65	4.75	2.45	3.95	8.14	5.07
Cs	4.93	5.10	5.48	4.87	10.81	6.24	18.45	4.52	13.45	9.05	2.11	3.78	8.56
Ta	0.32	0.47	0.76	0.26	0.11	0.38	0.41	0.39	0.47	0.52	0.33	0.49	0.44
Th/U	0.53	0.49	0.54	0.51	0.52	0.52	0.19	0.57	0.77	0.13	0.61	0.47	0.46
Y/Ho	74.2	74.69	76.32	74.44	75.49	75.03	434.18	149.61	43.1	16.27	120.47	212.69	162.7
Eu/Eu*	0.04	0.06	0.05	0.05	0.06	0.05	0.37	0.42	0.55	0.94	0.55	0.40	0.54
Ce/Ce*	1.24	1.24	1.31	1.24	1.27	1.26	1.26	0.68	1.35	1.44	12.25	35.97	8.82
Y/Y*	1.18	1.15	1.17	1.17	1.16	1.17	6.26	1.97	0.94	0.26	1.00	3.82	2.37
$(La/Lu)_N$	0.43	0.43	0.39	0.43	0.41	0.42	4.77	2.62	4.63	0.61	0.24	2.16	2.51
$(Gd/Lu)_N$	0.31	0.31	0.31	0.31	0.31	0.31	1.41	1.68	2.56	0.73	1.05	1.01	1.41
$(La/Sm)_N$	1.33	1.33	1.16	1.33	1.24	1.28	2.25	1.79	8.15	1.65	0.25	1.79	2.65
$(La/Yb)_N$	0.48	0.54	0.47	0.51	0.50	0.50	1.40	1.90	2.73	0.28	0.15	2.03	1.41
$(Tb/Yb)_N$	0.34	0.38	0.33	0.36	0.36	0.35	0.65	0.90	5	0.76	0.34	0.78	0.75

*The normalization is based on the chondrite-normalized data given by Sun and McDonough (1989): Eu anomaly is defined by $Eu/Eu^* = Eu_N/(\sqrt{Sm_N}^{\chi} Gd_N)$, Ce anomaly is defined by $Ce/Ce^* = Ce_N/(\sqrt{La_N}^{\chi} Pr_N)$, and Y anomaly is defined by $Y/Y^* = Y_N/(\sqrt{Er_N}^{\chi} Ho_N$

and Ti, while the traces such as Nb, La, Ce, Pr, Eu, and Yb show weak to moderate negative anomalies. This finding could be due to the fractionation of titanite, apatite, rutile, plagioclase, and K-feldspar, compared to the source history or magma. Nevertheless, the reduction of Ti, Sr, P, and Nb in the ErdSG indicates their derivation from crustal protolith (Elwan et al. 2019).

Tectonic setting and crystallization signatures

The 10^4 * Ga/Al (*) ratios in the ErdSG were found to be superior to the A-type granites global average (3.75) (Fig. 3A). ErdSG have the A-type granites (Fig. 3B) of ferroan signature (Fig. 3C) and a post-collisional tectonic setting (Fig. 3D) of A2 subgroup (Fig. 3E). These results could be ascribed to the partial melting of lower crust source via continent-continent (post-orogenic setting) or subduction collision. These findings were found in agreement with the reported results of other authors (Eby 1992; Blasy et al. 2001). In addition, there are several geochemical features suggesting that syenogranite is generated by partial melting of a crustal source such as the high Rb/Sr ratio (50.40, on average) and the restricted range of silica content which explain the limited crystal-liquid fractionation and the involvement of a crustal source (Wang et al. 2006).

Condition of crystallization signatures

ErdSG crystallization temperature was estimated by utilizing Al-Ti thermometer method which was explained by Jung and Pfänder (2007), whereas, the crystallization pressure and the emplacement depths were calculated by employing the barometer method (based on the determined crystallization pressures) proposed by Yang (2017).

The application of those thermobarometers reflects that ErdSG crystallization temperature and pressure ranging from 716.3 to 757.5 °C and from 1.71 to 1.95 kbars, respectively. This high crystallization temperature indicates that the granitic melts were highly fractionated (Chappell et al. 1998). Therefore, the aforementioned results revealed that fractional crystallization played a significant impact role in the derivation of ErdSG. Yang (2017) supposes that 1 kb (100 MPa) equals a depth of 2.7 km with an assumed continental crust density of 2.85 g/cm^3 and entirely lithostatic pressure. Accordingly, ErdSG were situated at depth ranges from 3.24 to 3.9 km. Furthermore, Huebner and Sato (1970) introduced the equilibrium expression which is used to calculate the oxygen fugacity buffers (log fO_2). Consequently, the oxidizing conditions of the ErdSG crystallization (log fO_2) were found in the range of − 7.12 to − 15.02. Moreover, the common occurrence of magnetites compared to other Fe-Ti oxide minerals in ErdSG (Abdel Warith et al. 2010) supports their crystallization under oxidizing conditions. Also, this finding reveals that ErdSG belongs to the series magnetite, whereas NNO fugacity buffer controls their crystallization as illustrated in Fig. 3F.

Fluorine contents and REEs tetrad effect

The highly evolved ErdSG shows M-type tetrad effect (Fig. 2K), that is mostly similar to the REEs tetrad effect produced

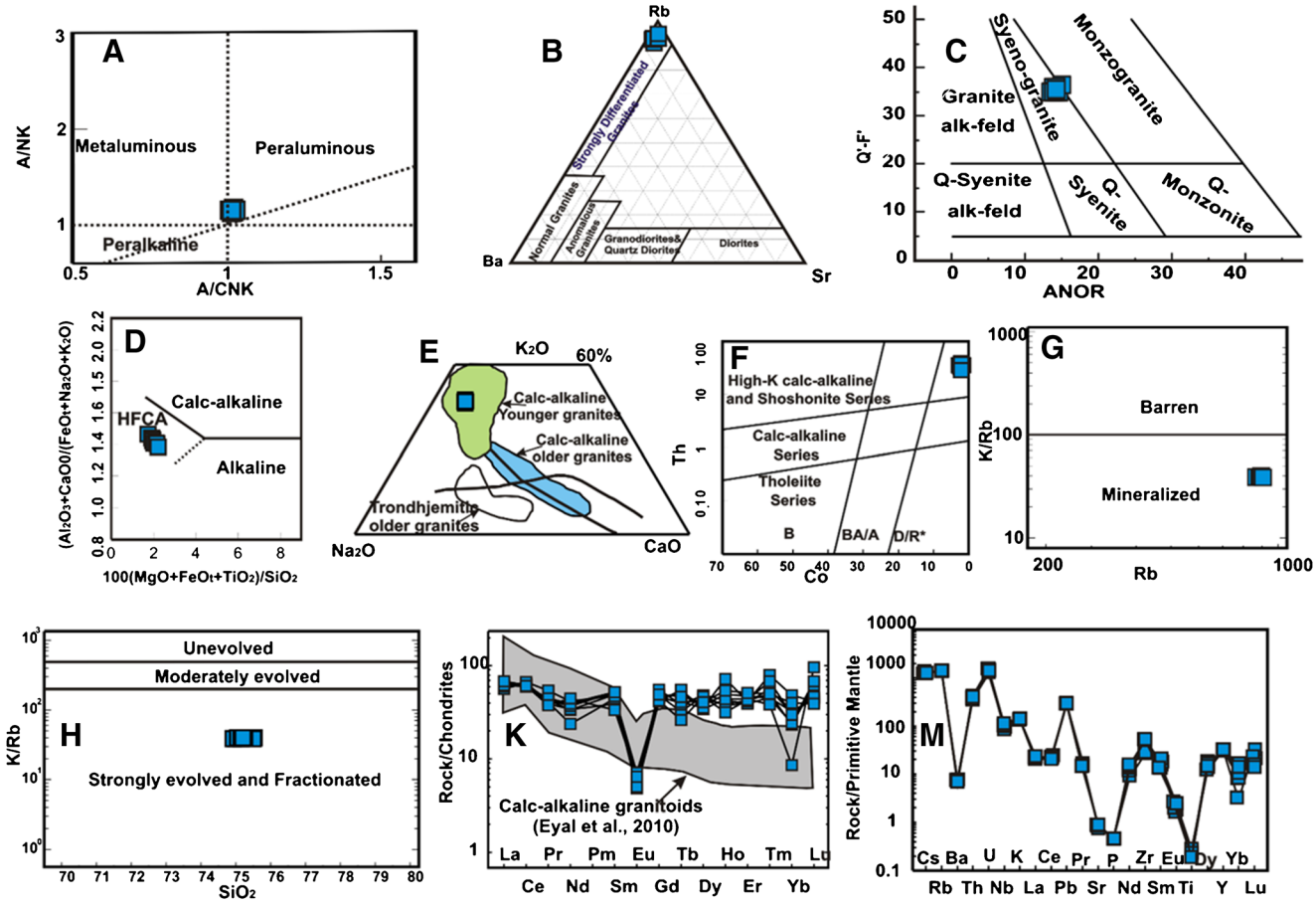

Fig. 2 Al_2O_3/ $CaO+Na_2O+K_2O$-Al_2O_3/Na_2O+K_2O diagram (after Maniar and Piccoli 1989) (**A**), Rb-Ba-Sr ternary diagram (after El Bouseily and El Sokkary 1975) (**B**), Q'- F'-ANOR diagram (after Streckeisen and Le Maitre 1979) (**C**), Al_2O_3+Cao/FeOt+Na_2O+K_2O vs. 100*(TiO_2+FeO_t+MgO)/SiO_2 diagram (after Sylvester 1989) (**D**), Na_2O-CaO-K_2O ternary diagram (after Hassan et al. 1990) (**E**), Co-Th diagram (after Hastie et al. 2007) (**F**), K/Rb - Rb diagram (after Tischendorf 1977) (**G**), K/Rb vs SiO_2 diagram (after Blevin 2003) (**H**), REE chondrite-normalized (comparable to calc-alkaline granitoids (Eyal et al. 2010) (**K**), and PM-normalized trace element patterns (**M**) for ErdYG (values after Sun and McDonough 1989)

in the F-rich highly differentiated granites from the Qianlishan composite plutons, S. China (Chen et al. 2014).

The behavior of charge- and radius-controlled (CHARAC) trace element overcomes in standard magmatic systems. However, the lanthanides tetrad effects are commonly associated with the non-CHARAC behaviors of trace elements (Bau 1996). In other words, in the geochemical system described by the behavior of non-CHARAC trace element, the elements of the same charge and radius (such as Y-Ho, Zr-Hf pairs) must be regulated by chemical complexation processes which cause trace elements fractionations (Bau 1996), which means that the stabilities of these controlled complexes are not restricted by particular charges and ionic radius of these individual elements (Mahdy et al. 2015). Similarly, this phenomenon was found in the magmatic systems (highly evolved), which characterized by a high amount of CO_2, H_2O, and other elements (such as B, Li, F, or/and Cl) that could be developed during late stage of granitoid crystallization among aqueous fluids and pure silicate melts (Bau 1996).

Figure 3G demonstrates that the ErdSG are following the non-CHARAC character. This behavior can be explained as the specific physicochemical features of the high-silica magmatic systems (Bau 1996), whereas the transitional characters happen among absolute silicate melts and hydrothermal fluids (Myint et al. 2017). The non-CHARAC trace element behavior and REEs tetrad effect are proportionate along with fluid-melt reactions during crystallization (Chen and Jahn 2004). The values of ErdSG tetrad effect (TE_{1-3}) were found in the range from 0.87 to 1.23 with a clearly visible tetrad pattern (Myint 2015). Accordingly, K/Rb ratios versus TE_{1-3} in the ErdSG (highly evolved) describe uncommon variations (Fig. 3H) compared to the normal magmatic rock ranges (common range of granitoids K/Rb ratios from 200 to 300) (Mahdy et al. 2015). Generally, these observations could be attributed to F-rich granitic magmas.

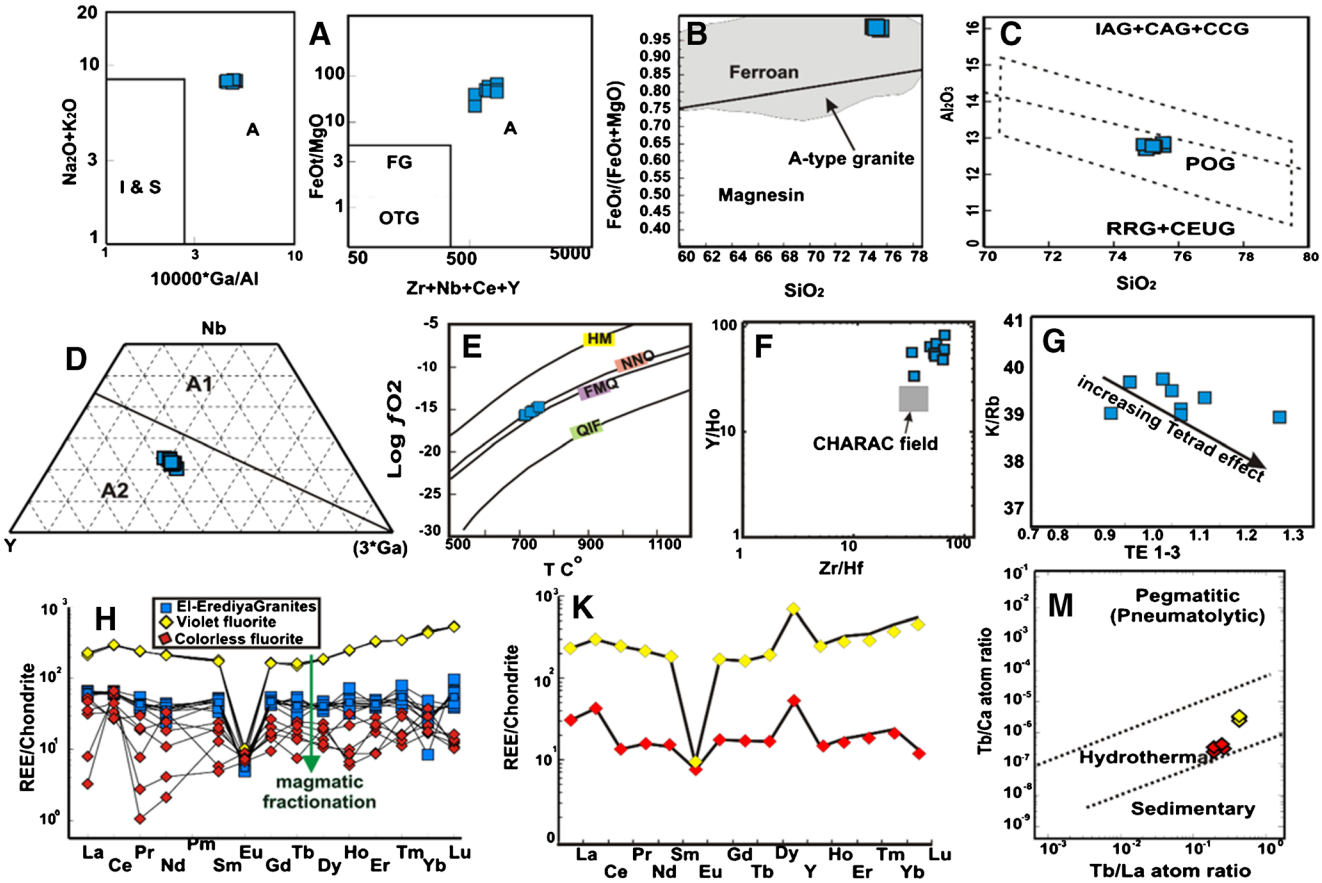

Fig. 3 Na_2O+K_2O-10,000 Ga/Al (**A**) and FeO_t/MgO-Zr+Nb+Ce+Y (**B**) discrimination diagrams (after Whalen et al. 1987), SiO_2 vs. FeO^t/FeO^t + MgO (Frost et al. 2001) (**C**), SiO_2-Al_2O_3 diagram (after Maniar and Piccoli 1989) (**D**), Nb-Y-3Ga triangular diagram of Eby 1992 (**E**), temperature vs. oxygen (*f*O2) fugacity diagram (**F**) for estimation the redox conditions (Wones 1989), HM (hematite-magnetite), NNO (nickel-nickel oxide), and QFM (quartz-fayalite-magnetite); Y/Ho-Zr/Hf diagram with charge- and radius-controlled (CHARAC) field (Bau 1996) (**G**), K/Rb-TE_{1-3} (degree of tetrad effect) of Irber 1999 (**H**), REE chondrite-normalized patterns of fluorites and ErdSG (normalization values after Sun and McDonough 1989) (**K**, **M**), and Variations of Tb/Ca-Tb/La ratios of the studied fluorite (Möller et al. 1976) (**N**)

Geochemistry of fluorite

Fluoritization is a predominant alteration of the ErdSG. Fluorite in the ErdSG varies from colorless to dark violet. The chemistry of fluorite (Table 2) clarified that the two types of fluorite (violet (VF) and colorless (CF)) have similar major constituents; however, there are differences in trace elements and REE contents. Both fluorite types contained high values of trace elements and REE. However, the VF contains a higher quantity of varied trace and REEs (Table 2).

The patterns of fluorite REE and trace elements could signify the source (melt or fluid) from which they originally precipitated or crystallized (Hill et al. 2000; Sallet et al. 2000). As already mentioned above, the ErdSG normalized REE patterns are described by relatively unfractionated flat patterns with strong negative Eu and Yb anomalies and weakly negative anomalies for Nd. The VF has higher concentrations of REE (ΣREE = 638.4) relative to the hosted granites (ΣREE = 120.99) and to the CF (ΣREE = 61.13) (Fig 3K; Table 2), with somewhat similar patterns. Both fluorites show higher value of LREE compared to HREE and exhibit strong negative Eu anomaly (Eu/Eu* = 0.05 and 0.54, respectively) with slight enrichment of Ce, Pr, Yb, Er, and La relative to the remaining REE members (Fig. 3M).

The fluorites REES enrichment related to host rock and the slight fractionation trend with inclined HREE suggest that hydrothermal-magmatic process occurs in granitic rocks (Schwinn and Markl 2005), whereas the hydrothermal fluids have a magmatic origin. Figure 3N supports the hydrothermal-magmatic process of fluorite formation.

The near resemblance of the chondrite-normalized REE patterns, superior LREEs content to HREEs content, and the enhancement in inconsistent lithophile elements (such as Ba, Th, Rb, Zr, Y, U, Nb, Pb) of ErdSG and hosted fluorites reflect the close relationship for both of them. In addition, the colorless fluorite REEs values that never exceed whole-rock values indicate their late origin from fluids equilibrated with already crystallized rock.

The present fluorite is marked by positive Y anomaly (Y/Y*Avg. = 1.17 and 2.37 for VF and CF, respectively)

and increasing Y/Ho ratio (Avg. 75.03 and 162.72 for VF and CF, respectively) (Table 2, Fig. 3M). As well, the mass balance of ErdSG indicated the losses of Y owing to the alterations and releasing of the accessory minerals from metamictized into the fluids (Mahdy et al. 2014). Specifically, the positively Y anomaly indicates robust complexation with F and decoupling of Y from HREE, which is a frequently occurred feature in fluids controlled by F complexes (Schönenberger et al. 2008). The increasing of Y/Ho ratio and positively Y anomalies of fluorites point out the interactivity with a fluorine-rich aqueous fluid.

Moreover, the REES concentrations in the magmatic-hydrothermal solutions are controlled by pH (raising with declining pH in the acidic solution; Honour et al. (2018)) and bulk compositions of the fluids. VF show a higher value of REES (Table 2) and $(La/Lu)_N$ ratio <1 compared to the CF $(La/Lu)_N$ ratio >1. These various patterns of fluorites from the same original source could indicate the robust influences of chemical complexation and physiochemical condition of leaching on the REE of source (Schwinn and Markl 2005). Similarly, the high LREEs concentration in studied fluorites suggests the transportation of fluorites as fluoride complexes in magmatic-hydrothermal system (Sheard et al. 2012).

The strong negative Eu anomalies of El-Erediya fluorites can be interpreted because of differences between the sizes of Eu^{2+} and Ca^{2+} ions (Schwinn and Markl 2005), which prevent substitution between these elements in the fluorite structure, especially at temperatures exceeding 200 °C. The crystallization temperature of the fluorite-bearing granitoids (~ 760 °C) supports the previous conclusion, where the Eu^{3+} is reduced to Eu^{2+} at T > 200 °C which prevents its incorporation into the fluorite crystal lattice. Hence, the fluorites show negatively Eu anomalies owing to the crystallographically dominated fractionation through the formation. Eu is mainly Eu^{2+} at fluorite crystallization temperatures from 390 to 430 °C (Sagiroglu 1984). Consequently, a strong negative Eu anomaly is expected in the types of fluorite produced at the high T conditions.

Fluid inclusions

The fluid inclusions in fluorite are small size (2–12 μm) and show that no micrometric evidence of CO_2 was found in any fluid inclusion; this suggests that a large amount of meteoric water diluted the secondary magmatic component (Fig. 4B). The inclusions are combined into two basic types Vis, I and II. The inclusions of type (I) are simple liquid-rich two-phase (liquid-vapor) inclusions. The inclusions of type (II) are liquid-rich three-phase (liquid-vapor-solid) inclusions (Fig. 4A). These inclusions in fluorite interpreted as a primary type according to the proposed criteria by Roedder (1984).

For the primary fluid inclusion examination (present study), homogenization temperatures (T_h) were observed ranging from 118 to 336 °C, which suggests fluorite crystallization at magmatic-hydrothermal transition conditions. The high homogenization temperatures and absence of CO_2 in the fluid inclusion clarified that U was transported in the magmatic-hydrothermal solutions as fluoride complex (El-Feky 2011). The fluoride complexes of U^{4+} and U^{6+}, at 200–300 °C, become vital at lower pH values for reducing-oxidizing conditions (Fayek et al. 2011).

Final ice melting (T_m) was observed during heating ranging from − 0.1 to − 12.1 °C with a corresponding salinity ranging from 0.18 to 16.05 wt.% NaCl equivalent (Table 3). Figure 4B illustrates the relationship (correlation) between salinity and homogenization temperature. The obtained result reveals that the magmatic-meteoric mixing fluid played the main role in fluid formation (Beane 1983). The plotted data of homogenization temperatures and salinities (Fig. 4C) were found in the field of epithermal deposit.

Petrogenetic aspects

The similarity of the El-Erediya highly differentiated granite to A-type granite can be inferred from (i) high Rb, Zr, SiO_2, Nb, Na_2O+K_2O, and Y contents; (ii) high 10000*Ga/Al and Rb/Sr ratios; (iii) low Ba/Rb, La/Nb, and Eu/Eu* ratios; (iv) weakly peraluminous and high K-calc-alkaline natures; and (v) depletion in MgO, CaO, TiO_2, P_2O_5, Sr, and Eu contents (Bau 1996). In addition, these Rb/Sr, Ba/Rb, La/Nb, and Eu/Eu* ratios in comparison with the lithospheric root suggest contributions of the lower crust and/or slab break off (Espinoza et al. 2005) at a depth greater than 30 km (Fig. 4D), which is further confirmed by multivariate segregation diagram (Fig. 4E) of Pearce and Gale (1977). Moreover, ErdSG are characterized by slightly peraluminous affinity (Fig. 2A, with average 0.19 % corundum in the norm) and are belonging to A_2 subtype (Fig. 3E) that is mostly emplaced in a post-orogenic setting and derived by arc crustal melting (Eby 1992). Thus, ErdSG are supposed to represent the post-orogenic granites, which are common in the Late-Precambrian of the ANS of Egypt (El-Sayed and Nisr 1999).

The Nb/Ta ratio in ErdSG (6.36–7.47) and Rb content (888.2–898.7 ppm) confirms that these granites have a magmatic-hydrothermal activity. The Nb/Ta ratio around 5 and Rb > 500 is commonly used as markers of magmatic-hydrothermal alterations in highly evolved crustal granite (Ballouard et al. 2015).

The U and Th concentrations and U/Th ratios suggest that the ErdSG melt was subjected to magmatic fractionation (Fig. 4F, G), reflecting the activities of post- to late-magmatic processes compared to exsolution of a fluid phase (Mahdy et al. 2015). In addition, the F and U are among the elements that tended to accumulate in the residual melts in the course of crystal differentiation (Keppler and Wyllie 1991). The low Sr and Ba and high Rb contents (Table 2) reveal that crystal fractionation was probable, the primary process driving

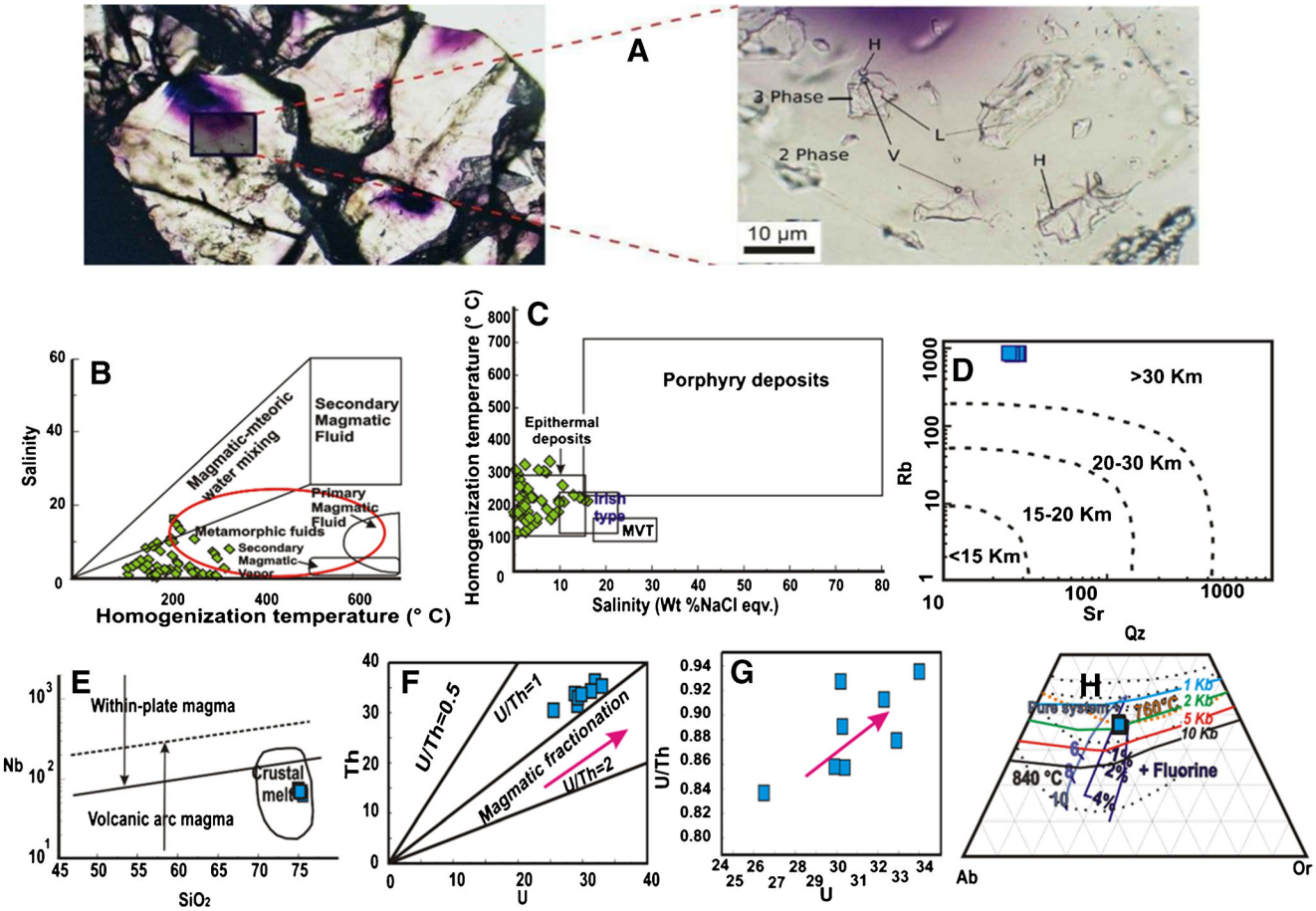

Fig. 4 Photomicrographs of fluid inclusions in fluorite show three phases H+V+L, and two phases (**A**); homogenization temperature versus salinity diagram for fluid inclusions (after Beane (1983)) (**B**); homogenization temperature-salinity diagram (after Wilkinson (2001)) (**C**); Rb-Sr variation diagram (Condie 1973) (**D**); SiO_2-Nb variation diagram proposed by Pearce and Gale (1977) (**E**); U-Th (**F**) and U-U/Th (**G**) diagrams (the trend after Cuney (2009)); normative An-Ab-Or ternary graph (**H**), temperature dotted lines (Barker 1979), the pressure solid lines (Johannes and Holtz 2012), and fluorine content (Manning 1981)

magma evolution. The limited variations in Al_2O_3, SiO_2, and high alkali contents, in addition to the Q-Or-Ab compositions, suggest that the syenogranite crystallization occurred close to the minimum in granite system (Christiansen and Lee 1986). Furthermore, the significant ErdSG ratios such as Eu/Eu* < 0.2, Ca/Sr > 113, Rb/Sr > 4.4, Rb/Ba > 0.6, and K/Ba > 113 indicate that first fractionation of plagioclase and K-feldspar was presently significant in this least fractionated unit.

Role of fluorine-rich magma

F is such a good oxidizing agent that replaces O in fluids/melts or minerals and may change the valency of U from U^{4+} to U^{6+} and may form soluble fluoride or hydroxyl-fluoride complexes. The common association of U and fluorite suggests that U was transported as U-F complex. In addition, F-bearing minerals (i.e., fluorite) showed a capability to transfer otherwise fluid-immobile trace elements. This observation was confirmed by the existence of REE-bearing minerals in the granite such as fluorite, zircon, monazite, allanite, and apatite. Additionally, Fig. 4H shows that ErdSG samples were plotted close to the minimum melt composition (in the Qz-Ab-Or-H_2O-F haplogranite system) in the existence of fluorine at temperature ≈ 760 °C and pressure ≈ 2 kbar.

According to the obtained geochemical data, the ErdSG were generated by fractional crystallization processes (Ismael and Kharbish 2013). Besides, volatile transfer mechanisms showed a significant effect during the evolution of the studied granites. Therefore, fluorine is considered as one of the most important elements in the fluid phase, which could be clearly inferred by the extensive occurrence of fluorite among the other accessory minerals in syenogranite. Generally, the high F contents in the magmas largely enhance the mobility of HFSE (Jiang et al. 2005). Commonly, alkali-fluoro complexes are formed from fluorine-rich magmas, Ga, Y, Zr, Nb, and REE (White et al. 1982), these complexes showing more stability in the melt (Mohamed and El-Sayed 2008). During the late stages of magmatic evolution, these complexes will also be precipitated. This precipitation behavior could be ascribed to the relatively low amount of water contents at these late

Table 3 Microthermometric data of primary fluid inclusions within fluorite of the El-Erediya granite

No	Tm	Phase	Th_{L-V}	wt% NaCl
1	− 1.6	Ice	250	2.74
2	− 1.3	Ice	259	2.24
3	− 1	Ice	265	1.74
4	− 1	Ice	268	1.74
5	− 0.7	Ice	281	1.22
6	− 0.5	Ice	297	0.88
7	− 0.3	Ice	307	0.53
8	− 0.3	Ice	308	0.53
9	− 0.3	Ice	309	0.53
10	− 7.4	Ice	212	10.98
11	− 6.5	Ice	216	9.86
12	− 2.6	Ice	225	4.34
13	− 2.3	Ice	226	3.87
14	− 1.8	Ice	252	3.06
15	− 0.8	Ice	258	1.40
16	− 12.1	Ice	216	16.05
17	− 11.3	Ice	220	15.27
18	− 10.5	Ice	224	14.46
19	− 10.4	Ice	225	14.36
20	− 9.3	Ice	231	13.18
21	− 7.1	Ice	261	10.61
22	− 4.5	Ice	302	7.17
23	− 4.2	Ice	306	6.74
24	− 3.3	Ice	310	5.41
25	− 1.5	Ice	326	2.57
26	− 5	Ice	336	7.86
27	− 0.5	Ice	120	0.88
28	− 1.25	Ice	160	2.16
29	− 1	Ice	198	1.74
30	− 1.25	Ice	225	2.16
31	− 0.2	Ice	170	0.35
32	− 0.1	Ice	180	0.18
33	− 1.5	Ice	118	2.57
34	− 1.8	Ice	129	3.06
35	− 2.3	Ice	138	3.87
36	− 0.6	Ice	178	1.05
37	− 1.7	Ice	155	2.90
38	− 3.8	Ice	214	6.16
39	− 1.4	Ice	211	2.41
40	− 2.9	Ice	148	4.80
41	− 5.2	Ice	159	8.14
42	− 3.1	Ice	163	5.11
43	− 6.4	Ice	183	9.73
44	− 5.6	Ice	173	8.68
45	− 4.6	Ice	188	7.31
46	− 6.6	Ice	207	9.98
47	− 1.6	Ice	153	2.74
48	− 1.8	Ice	182	3.06
49	− 2.1	Ice	161	3.55
50	− 0.7	Ice	222	1.22
51	− 1.2	Ice	203	2.07
52	− 1	Ice	184	1.74
53	− 1.4	Ice	199	2.41

stages (Collins et al. 1982). The structure of the melt is highly controlling the tendency of HFSE to produce fluoro complexes with high stability (Charoy and Raimbault 1994). The magmatic differentiation could be promoted owing to the high activity of F, which improves the crystal fractionation rate. Moreover, F-rich fluids are extremely useful in the transport of HFSE in the form of fluorinated complexes (Mohamed and El-Sayed 2008; Maged et al. 2020a). Figure 5 illustrates the correlation between F and Nb, Zr, Rb, Y, and REEs of the studied ErdSG; the obtained results showed that positive correlation occurred. These findings were found in agreement with hypothesis of F-complexing of the mentioned elements and their resultant mobility during the granite evolution. The ErdSG considered as strongly evolved and fractionated high-fluorine silicic rocks (HFSR), where the fluorine performed an important role in enriching U in late-stage hydrothermal-magmatic fluids. The average Th/U ratio in fluorite and syenogranite reflects that the rock units suffering post-magmatic process result in mobilization of U relative to Th, which is suitable for leaching.

U-F mineralization

ErdYG has a U content (Avg. 29.8 ppm) more than the Clark value (4 ppm) [uraniferous granites are defined as any granitic masses containing U at least twice the Clark value (4 ppm)]. Uranium is mainly found as a complex compound bonded with fluorine in high-temperature magma-hydrothermal systems (Rich et al. 1977). Fluorine tends to cause changes in the liquidus phase and also able to break the bridging oxygen bonds causing melt depolymerization, consequently increasing the U solubility in the magma (Peiffert et al. 1996; Mysen et al. 2004). The partition coefficients of F between fluid and magma are low (approximately 0.2–0.1). As a result, F concentrates in magma and joins in the crystal lattice of biotites and apatites phases. However, syenogranite contains small amounts of apatite as an accessory mineral, biotite as essential mineral, and muscovite occurs only in altered zones of granites as a secondary mineral formed in the post-magmatic

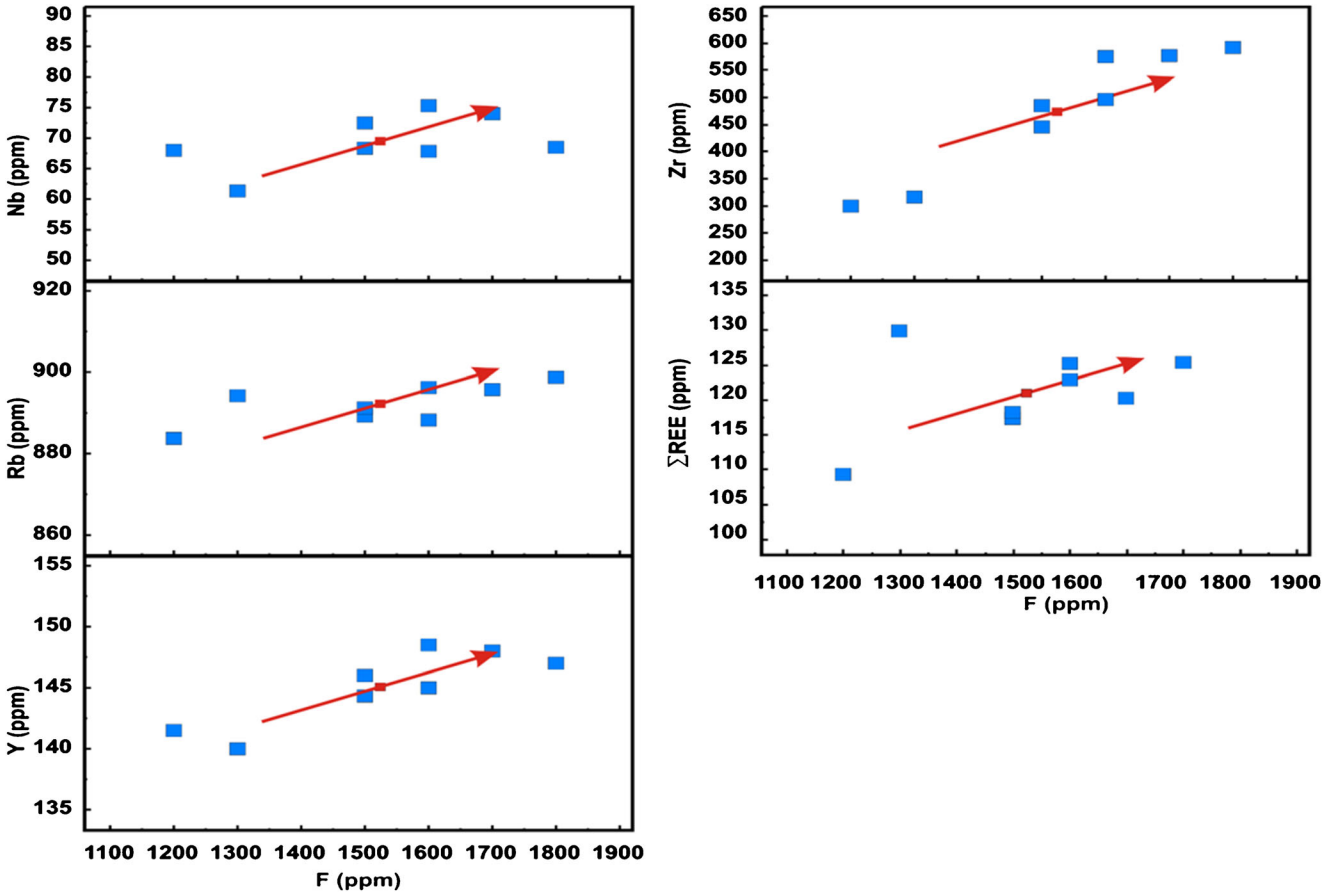

Fig. 5 Variation of F vs. Nb, Rb, Y, Zr, and REE of the studied ErdSG

stages through the hydrolysis of K-feldspars (Mahdy 2011; Maged et al. 2020b). So, syenogranites are highly evolved F-enriched granites (Abdel Warith et al. 2010). Accordingly, the developments of the fluorine of granitic magma of syenogranites are either by the formation of its own minerals or within magmatic cupolas during fractionation processes.

The partition coefficients of uranium between fluid and magma are much lower in fluorine-rich magmas, varying from (3×10^{-2}) to (4×10^{-2}) (Chabiron et al. 2003). As a result, F-enriched magmas tend to have much higher U concentrations (Lui and Lui 2009). U-rich fluorite in syenogranite occurs as small disseminations in fresh zones of host granites and mainly filling the fractures as veinlets in the altered zones of G. El-Erediya host granites.

Conclusions

The above discussion postulates that: The ErdSG are considered as high-fluorine silicic rocks (HFSR), where the fluorine performed an important role in enriching U in late-stage hydrothermal-magmatic fluids. Fluorite is an important indicator for U mineralization. The fluorine is the main factor for the enriching of uranium in the late-stage hydrothermal-magmatic fluids. Eight representative granite samples have been collected in El-Erediya area in order to determine the origin, geochemical behavior, petrochemical characteristics, mineralization, and their tectonic settings. Eleven fluorite samples were analyzed (electron microprobe analyses) to clarify the environment of formation and its relation to U mineralization. The results of the analyzed samples can be concluding as follows:

1. Syenogranits are strongly evolved and fractionated granites with high-fluorine content.
2. They are mineralized granites, slightly peraluminous, derive from highly K-calc-alkaline magma with potassic affinity and emplaced as post-orogenic granitoids.
3. They are highly differentiated granite, considered as A2-type granites, which are derivatives of basaltic/amphibolitic sources underplating in the lower crust.
4. They are considered as uraniferous granite and favorable for U mineralization.
5. The fluorite is formed and concurrent with the uranium mineralization, showing that the source of the uranium is the hosted granite, which is transported as U-fluoride complex. The solubility of the U in the hydrothermal

solutions is mainly controlled by the fluoride complex formation.

6. The fluorine is the main factor for the remobilization and enrichment of U in the hydrothermal solutions. The U-rich granite subjected to tectonic and hydrothermal processes causing alterations of rock-forming minerals. These processes are mostly responsible for U concentration and its redistribution, which form U-rich fluorite mineralization along cavities and fractures in granite hosted rocks.
7. Fluorite varies from colorless to dark violet in color. They recorded high U content.
8. The average Th/U ratio in colorless and violet fluorite type (Avg. 0.46 and 0.52, respectively) and syenogranite (Avg. 1.13) is less than 3 and appears that rock units suffering post-magmatic process result in mobilization of uranium relative to thorium, which is suitable for leaching.
9. The minimal temperature of fluorites origin can be estimated from the homogenization temperatures of primary fluid inclusions in fluorites (118 and 336 °C); also, they have high REE contents related to a hydrothermal-magmatic system.

Finally, it can be concluded that the syenogranite considered as HFSR, which included two types of fluorites according to their U and REE contents. The colorless fluorite is poor in U and REE, relative to the violet type, which is rich in U, and REE. The F-enriched granite can be considered as fertile and possess the same chemical characteristic parameter of fertile granite.

Acknowledgements The authors are grateful to Dr. M. **Götzinger** for his kind help during the fluid inclusion measurements. The authors sincerely express their appreciation and thanks to the editor and reviewers whose critical commentary has significantly improved the quality of this publication.

Author contribution **Dr. Omar Amer:** Conceptualization, visualization, writing-original draft

Prof. Dr. Sherif Kharbish: Conceptualization, project administration, formal analysis, review and editing

Dr. Ali Maged: Conceptualization, writing-original draft, visualization, review and editing

Dr. Fares Khedr: Project administration, visualization, writing

Declarations

Conflict of interest The authors declare no competing interests.

References

Abdel Warith A, Michalik M, Ali BH (2010) Fluorine enriched granites: chemical characterization and relation to uranium mineralization. J Appl Sci Res 6:299–323

Abu Dief A (1993) The relation between the uranium mineralization and tectonics in some Pan-African granite, west of Safaga, Eastern Desert, Egypt. (Ph.D. Thesis). Assuit University

Aleshin A, Velichkin V, Cuney M, et al (2002) Ontogeny and typomorphic features of uranium mineralization at Mo-U deposits of the Streltsovskaya caldera (Transbaikalia, Russia). In: In Proceedings of the international workshop'Uranium deposits: from their genesis to their environmental aspects. pp 29–32

Aleshin A, Velichkin V, Krylova T (2007) Genesis and formation conditions of deposits in the unique Strel'tsovka molybdenum-uranium ore field: new mineralogical, geochemical, and physicochemical. Geol Ore Depos 49:392–412. https://doi.org/10.1134/S1075701507050054

Bakhit FS, El Kassas IA (1989) Distribution and orientation of radioactive veins in the El Erediya-El Missikat area, Central Eastern Desert, Egypt. Int J Remote Sens 10:565–581. https://doi.org/10.1080/01431168908903893

Ballouard C, Poujol M, Boulvais P et al (2015) Is the Nb-Ta fractionation a marker of an interaction with fluids in peraluminous granites? In: GA2015: 13th Biennial meeting. Nancy, France, pp 675–678

Barker F (1979) Trondhjemite: Definition, environment and hypotheses of origin. Developments in Petrology. Elsevier, pp 1–12

Bau M (1996) Controls on the fractionation of isovalent trace elements in magmatic and aqueous systems: evidence from Y/Ho, Zr/Hf, and lanthanide tetrad effect. Springer-Verlag

Beane RE (1983) The magmatic-meteoric transition. Geotherm Resour Counc Spec Rep 13:245–253

Beyth M, Stern RJ, Altherr R, Kröner A (1994) The Late Precambrian Timna igneous complex, southern Israel: evidence for comagmatic-type sanukitoid monzodiorite and alkali granite magma. LITHOS 31:103–124. https://doi.org/10.1016/0024-4937(94)90003-5

Blasy M, Baroudy AF, Kharbish SM (2001) Geochemical characteristics of Wadi Tarr albitite, Southeastern Sinai, Egypt. Egypt J Geol 42: 767–780

Blevin PL (2003) Metallogeny of granitic rocks. In: Magmas to mineralisation: the Ishihara Symposium, vol 14, Blevin P, Jones M, Chappell B edn. Ishihara Symp GEMOC, Macquarie Univ, p 155

Chabiron A, Michel AE, Ae C, Poty B (2003) Possible uranium sources for the largest uranium district associated with volcanism: the Streltsovka caldera (Transbaikalia, Russia). Springer 38:127–140. https://doi.org/10.1007/s00126-002-0289-0

Chappell BW, Bryant CJ, Wyborn D et al (1998) High- and low-temperature I-type granites. Resour Geol 48:225–235. https://doi.org/10.1111/j.1751-3928.1998.tb00020.x

Charoy B, Raimbault L (1994) Zr-, Th-, and REE-rich biotite differentiates in the A-type granite pluton of Suzhou (Eastern China): the key role of fluorine. J Petrol 35:919–962. https://doi.org/10.1093/petrology/35.4.919

Chen B, Jahn BM (2004) Genesis of post-collisional granitoids and basement nature of the Junggar Terrane, NW China: Nd-Sr isotope and trace element evidence. J Asian Earth Sci 23:691–703. https://doi.org/10.1016/S1367-9120(03)00118-4

Chen YW, Bi XW, Hu RZ, Dong SH (2012) Element geochemistry, mineralogy, geochronology and zircon Hf isotope of the Luxi and Xiazhuang granites in Guangdong province, China: Implications for U mineralization. Lithos 150:119–134. https://doi.org/10.1016/j.lithos.2012.06.025

Chen B, Ma X, Wang Z (2014) Origin of the fluorine-rich highly differentiated granites from the Qianlishan composite plutons (South China) and implications for polymetallic mineralization. J Asian Earth Sci 93:301–314. https://doi.org/10.1016/j.jseaes.2014.07.022

Christiansen EH, Lee DE (1986) Fluorine and chlorine in granitoids from the Basin and Range province, western United States. Econ Geol 81: 1484–1494. https://doi.org/10.2113/gsecongeo.81.6.1484

Collins WJ, Beams SD, White AJR, Chappell BW (1982) Nature and origin of A-type granites with particular reference to southeastern Australia. Contrib Mineral Petrol 80:189–200

Condie KC (1973) Archean magmatism and crustal thickening. Bull Geol Soc Am 84:2981–2992. https://doi.org/10.1130/0016-7606(1973)84<2981:AMACT>2.0.CO;2

Cuney M (2009) The extreme diversity of uranium deposits. Mineral Deposita 44:3–9. https://doi.org/10.1007/s00126-008-0223-1

Cuney M (2014) Felsic magmatism and uranium deposits. Bull Soc Geol Fr 185:75–92. https://doi.org/10.2113/gssgfbull.185.2.75

Eby GN (1992) Chemical subdivision of the A-type granitoids: petrogenetic and tectonic implications. Geology 20:641–644. https://doi.org/10.1130/0091-7613(1992)020<0641:CSOTAT>2.3.CO;2

El Bouseily AM, El Sokkary AA (1975) The relation between Rb, Ba and Sr in granitic rocks. Chem Geol 16:207–219. https://doi.org/10.1016/0009-2541(75)90029-7

El-Feky MG (2011) Mineralogical, REE-geochemical and fluid inclusion studies on some uranium occurrences, Gabal Gattar, Northeastern Desert, Egypt. Chin J Geochem 30:430–443. https://doi.org/10.1007/s11631-011-0529-z

El-Sayed MM, Nisr SA (1999) Petrogenesis and evolution of the Dineibit El-Qulieb hyperaluminous leucogranite, Southeastern Desert, Egypt: petrological and geochemical constraints. J Afr Earth Sci 28:703–720. https://doi.org/10.1016/S0899-5362(99)00040-8

Elwan W, Azzaz SA, Balasi MR, Amer O (2019) Petrogenesis of Maktali fractionated calc-alkaline younger granitoids, Central Eastern Desert, Egypt. Arab J Geosci 12:1–17. https://doi.org/10.1007/s12517-019-4559-x

Espinoza F, Morata D, Pelleter E, Maury RC, Suárez M, Lagabrielle Y, Polvé M, Bellon H, Cotten J, de la Cruz R, Guivel C (2005) Petrogenesis of the Eocene and Mio-Pliocene alkaline basaltic magmatism in Meseta Chile Chico, southern Patagonia, Chile: evidence for the participation of two slab windows. Lithos 82:315–343. https://doi.org/10.1016/j.lithos.2004.09.024

Eyal M, Litvinovsky B, Jahn BM, Zanvilevich A, Katzir Y (2010) Origin and evolution of post-collisional magmatism: coeval Neoproterozoic calc-alkaline and alkaline suites of the Sinai Peninsula. Chem Geol 269:153–179. https://doi.org/10.1016/j.chemgeo.2009.09.010

Fayek M, Horita J, Ripley EM (2011) The oxygen isotopic composition of uranium minerals: a review. Ore Geol Rev 41:1–21

Fritz H, Abdelsalam M, Ali KA, Bingen B, Collins AS, Fowler AR, Ghebreab W, Hauzenberger CA, Johnson PR, Kusky TM, Macey P, Muhongo S, Stern RJ, Viola G (2013) Orogen styles in the East African orogen: a review of the Neoproterozoic to Cambrian tectonic evolution. J Afr Earth Sci 86:65–106. https://doi.org/10.1016/j.jafrearsci.2013.06.004

Frost BR, Barnes CG, Collins WJ et al (2001) A geochemical classification for granitic rocks. J Petrol 42:2033–2048. https://doi.org/10.1093/petrology/42.11.2033

Ghoneim MM, Gawad AA (2018) Vein-type uranium mineralization in the Eastern Desert of Egypt. News Ural State Min Univ 1:33–38

Hassan MA, Hashad AH, Said R (1990) The geology of Egypt Precambrian of Egypt. Routledge

Hastie AR, Kerr AC, Pearce JA, Mitchell SF (2007) Classification of altered volcanic island arc rocks using immobile trace elements: development of the Th–Co discrimination diagram. J Petrol 48:2341–2357. https://doi.org/10.1093/petrology/egm062

Hill GT, Campbell AR, Kyle PR (2000) Geochemistry of southwestern New Mexico fluorite occurrences implications for precious metals exploration in fluorite-bearing systems. J Geochem Explor 68:1–20. https://doi.org/10.1016/S0375-6742(99)00047-3

Honour VC, Goodenough KM, Shaw RA, Gabudianu I, Hirtopanu P (2018) REE mineralisation within the Ditrău Alkaline Complex, Romania: interplay of magmatic and hydrothermal processes. Lithos 314–315:360–381. https://doi.org/10.1016/j.lithos.2018.05.029

Huebner J, Sato M (1970) The oxygen fugacity-temperature relationships of manganese oxide and nickel oxide buffers. Am Mineral J Earth Planet Mater 55:934–952

IAEA (2012) World distribution of uranium deposits (UDEPO) with uranium deposit classification. Int At Energy Agency 117.

Ibrahim ME, Saleh GM, Abd El-Naby HH (2001) Uranium mineralization in the two mica granite of Gabal Ribdab area, South Eastern Desert, Egypt. Appl Radiat Isot 55:861–872. https://doi.org/10.1016/s0969-8043(01)00122-1

Ibrahim T, Cuney M, El Agami N et al (2004) Alteration processes and elements mobilIty in el missikat granite. In: Intern. Conf On Geochemistry. Alex.Univ, Egypt, pp 465–481

Ibrahim M, Watanabe K, Saleh G, Ibrahim W (2015) Abu Rusheid lamprophyre dikes, South Eastern Desert, Egypt: as physical-chemical traps for. Arab J Geosci 8:9261–9270. https://doi.org/10.1007/s12517-015-1882-8

Irber W (1999) The lanthanide tetrad effect and its correlation with K/Rb, Eu/Eu*, Sr/Eu, Y/Ho, and Zr/Hf of evolving peraluminous granite suites. Geochim Cosmochim Acta 63:489–508. https://doi.org/10.1016/S0016-7037(99)00027-7

Ismael IS, Kharbish S (2013) Removing of as (V) from aqueous solution using natural and pretreated glauconite and halloysite. Carpathian J Earth Environ Sci 8:187–198

Jiang SY, Wang RC, Xu XS, Zhao KD (2005) Mobility of high field strength elements (HFSE) in magmatic-, metamorphic-, and submarine-hydrothermal systems. Phys Chem Earth 30:1020–1029. https://doi.org/10.1016/j.pce.2004.11.004

Johannes W, Holtz F (2012) Petrogenesis and experimental petrology of granitic rocks. Springer Science & Business Media

Jung S, Pfänder JA (2007) Source composition and melting temperatures of orogenic granitoids: constraints from CaO/Na2O, Al2O3/TiO2 and accessory mineral saturation thermometry. Eur J Mineral 19:859–870. https://doi.org/10.1127/0935-1221/2007/0019-1774

Keppler H, Wyllie PJ (1991) Partitioning of Cu, Sn, Mo, W, U, and Th between melt and aqueous fluid in the systems haplogranite-H2O-HCl and haplogranite-H2O-HF. Contrib Mineral Petrol 109:139–150. https://doi.org/10.1007/BF00306474

Kharbish S (2010) Geochemistry and magmatic setting of Wadi El-Markh island-arc gabbro-diorite suite, central Eastern Desert, Egypt. Chem Erde 70:257–266. https://doi.org/10.1016/j.chemer.2009.12.007

Kharbish S (2020) Mineral chemistry, geochemistry, Raman spectroscopy and geotectonic significance of Neoproterozoic ophiolitic peridotites and pyroxenites from Kab Amiri district, central Eastern Desert, Egypt. Front Sci Res Technol 0:0–0. https://doi.org/10.21608/fsrt.2020.19309.1002

Kharbish S, Elawadi A (2018) Geochemistry and geotectonic significance of neoproterozoic ophiolitic peridotites and pyroxenites: KAB AMIRI, EASTERN DESERT, EGYPT Mineralogy and physico-chemical properties of Wadi Badaa clays (Cairo-Suez district, Egypt): a prospective resource for th. ACTA Univ MATTHIAE BELII Ser Environ Manag XX 1:38–45. 10.24040/actaem.2018.20.1.38-45

Kharbish S, El-Awady A (2019) Geochemical, mineralogical and petrogenetic studies of the calc-alkaline younger gabbros, Sinai of Egypt with a special emphasis on the role of hydrous fluids. J Afr Earth Sci 155:13–31. https://doi.org/10.1016/j.jafrearsci.2019.04.002

Kharbish S, Raslan MF, Raslan MF et al (2021) Occurrence of polymetallic mineralized pegmatite at Wadi El Sheih granite, Central Eastern Desert, Egypt. IOSR J Appl Geol Geophys 9:1–18. https://doi.org/10.9790/0990-0902010118

Kovalenko VI (1971) Topaz-bearing quartz keratophyre (ongonite), a new variety of subvolcanic igneous vein rock. Trans USSR Acad Sci, Earth Sci Sec 199:132–135

Lambert I, Jaireth S, McKay A, Miezitis Y (2005) Why Australia has so much uranium. AUSGEO news 80:7–10

Lui ZY, Lui HX (2009) The simulation test of granite uranium mineralization. Earth Sci Front 16:99–113

Maged A, Ismael ISIS, Kharbish S et al (2020a) Enhanced interlayer trapping of Pb(II) ions within kaolinite layers: intercalation, characterization, and sorption studies. Environ Sci Pollut Res 27:1870–1887. https://doi.org/10.1007/s11356-019-06845-w

Maged A, Kharbish S, Ismael ISIS, Bhatnagar A (2020b) Characterization of activated bentonite clay mineral and the mechanisms underlying its sorption for ciprofloxacin from aqueous solution. Environ Sci Pollut Res 27:1–18. https://doi.org/10.1007/s11356-020-09267-1

Mahdy NM (2011) Mineralogical studies and mineral chemistry of some radioactive mineralizations in Gabal Gattar area, Northern Eastern Desert. Ain Shams University, Egypt

Mahdy NM, Shalaby MH, Helmy HM, Osman AF, el Sawey ESH, Zeid EKA (2014) Trace and REE element geochemistry of fluorite and its relation to uranium mineralizations, Gabal Gattar Area, Northern Eastern Desert, Egypt. Arab J Geosci 7:2573–2589. https://doi.org/10.1007/s12517-013-0933-2

Mahdy NM, El Kalioubi BA, Wohlgemuth-Ueberwasser CC et al (2015) Petrogenesis of U- and Mo-bearing A2-type granite of the Gattar batholith in the Arabian Nubian Shield, Northeastern Desert, Egypt: evidence for the favorability of host rocks for the origin of associated ore deposits. Ore Geol Rev 71:57–81. https://doi.org/10.1016/j.oregeorev.2015.05.001

Maniar PD, Piccoli PM (1989) Tectonic discrimination of granitoids. Geol Soc Am Bull 101:635–643. https://doi.org/10.1130/0016-7606(1989)101<0635:TDOG>2.3.CO;2

Manning DAC (1981) Contributions to mineralogy and petrology the effect of fluorine on liquidus phase relationships in the system Qz-Ab-Or with excess water at 1 kb

Mohamed FH, El-Sayed MM (2008) Post-orogenic and anorogenic A-type fluorite-bearing granitoids, Eastern Desert, Egypt: petrogenetic and geotectonic implications. Chem Erde 68:431–450. https://doi.org/10.1016/j.chemer.2007.01.001

Möller P, Parekh PP, Schneider HJ (1976) The application of Tb/Ca-Tb/La abundance ratios to problems of fluorspar genesis. Mineral Deposita 11:111–116. https://doi.org/10.1007/BF00203098

Moussa EM (2006) Post collisional a-type granites at Al Missikat and Al Aradiya, Central Eastern Desert, Egypt: geochemical characteristics and REE petrogenetic modeling. In: In Proceedings of the 7th International Conference on Geochemistry. Alex. University, Egypt, pp 1–16

Myint A (2015) Granite-related Sn-W-Ree mineralization of Mawchi and Dawei areas. Kyushu University, Myanmar

Myint AZ, Zaw K, Swe YM et al (2017) Geochemistry and geochronology of granites hosting the Mawchi SN-W deposit, Myanmar: implications for tectonic setting and emplacement. Geological Society Memoir. Geological Society of London, pp 385–400

Mysen BO, Cody GD, Smith A (2004) Solubility mechanisms of fluorine in peralkaline and meta-aluminous silicate glasses and in melts to magmatic temperatures. Geochim Cosmochim Acta 68:2745–2769. https://doi.org/10.1016/j.gca.2003.12.015

Nash WP (1993) Fluorine iron biotite from the honeycomb hills rhyolite, Utah: the halogen record of decompression in a silicic magma. Am Mineral 78:1031–1040

Odikadze GL (1971) Distribution of fluorine in the granitoids of the great Caucasus and Dzirul massif. Geokhimiya 5:523–533

Pearce JA, Gale GH (1977) Identification of ore-deposition environment from trace-element geochemistry of associated igneous host rocks. Geol Soc Spec Publ 7:14–24. https://doi.org/10.1144/GSL.SP.1977.007.01.03

Peiffert C, Nguyen-Trung C, Cuney M (1996) Uranium in granitic magmas: Part 2. Experimental determination of uranium solubility and fluid-melt partition coefficients in the uranium oxide-haplogranite-H2O-NaX (X = Cl, F) system at 770°C, 2 kbar. Geochim Cosmochim Acta 60:1515–1529. https://doi.org/10.1016/0016-7037(96)00039-7

Rich R, Bailey DK, Macdonald R, Powell BN (1977) Hydrothermal uranium deposits. Dev Econ Geol 6:361–362

Roedder E (1984) Fluid inclusions: reviews in mineralogy. Mineral Soc Am Washingt DC 12.

Rossi JN, Toselli AJ, Basei MA, Sial AN, Baez M (2011) Geochemical indicators of metalliferous fertility in the Carboniferous San Blas pluton, Sierra de Velasco, Argentina. Geol Soc Spec Publ 350: 175–186. https://doi.org/10.1144/SP350.10

Sagiroglu A (1984) Akdagmadeni (Yozgat) kontakt metasomatik yataklarinda sivi kapanim çalişmalari. Akdagmadeni kontakt metasomatik yataklarinda sivi kapanim çalişmalari 27

Saleh GM, Kamar MS (2018) Geochemical characteristics and radioactive elements estimation along trenches of Um Ara area, South Eastern Desert. Egypt Geoinformatics Geostatistics An Overv 06. https://doi.org/10.4172/2327-4581.1000178

Sallet R, Moritz R, Fontignie D (2000) Fluorite 87Sr/86Sr and REE constraints on fluid-melt relations, crystallization time span and bulk D(Sr) of evolved high-silica granites. Tabuleiro granites, Santa Catarina, Brazil. Chem Geol 164:81–92. https://doi.org/10.1016/S0009-2541(99)00143-6

Schönenberger J, Köhler J, Markl G (2008) REE systematics of fluorides, calcite and siderite in peralkaline plutonic rocks from the Gardar Province, South Greenland. Chem Geol 247:16–35. https://doi.org/10.1016/j.chemgeo.2007.10.002

Schwinn G, Markl G (2005) REE systematics in hydrothermal fluorite. Chem Geol 216:225–248. https://doi.org/10.1016/j.chemgeo.2004.11.012

Sheard ER, Williams-Jones AE, Heiligmann M, Pederson C, Trueman DL (2012) Controls on the concentration of zirconium, niobium, and the rare earth elements in the Thor Lake rare metal deposit, Northwest Territories, Canada. Econ Geol 107:81–104. https://doi.org/10.2113/econgeo.107.1.81

Streckeisen A, Le Maitre R (1979) A chemical approximation to the modal QAPF classification of the igneous rocks. Miner Abh 136: 169–206

Sun SS, McDonough WF (1989) Chemical and isotopic systematics of oceanic basalts: Implications for mantle composition and processes. Geol Soc Spec Publ 42:313–345. https://doi.org/10.1144/GSL.SP.1989.042.01.19

Sylvester PJ (1989) Post-collisional alkaline granites. J Geol 97:261–280. https://doi.org/10.1086/629302

Tischendorf G (1977) Geochemical and petrographic characteristics of silicic magmatic rocks associated with rare-element mineralization. Stemprok, M, Burn L Tischendorf, G, Met Assoc with acid Magmat 2:41–98

Wang Q, Wyman DA, Xu JF, Zhao ZH, Jian P, Xiong XL, Bao ZW, Li CF, Bai ZH (2006) Petrogenesis of Cretaceous adakitic and shoshonitic igneous rocks in the Luzong area, Anhui Province (eastern China): Implications for geodynamics and Cu-Au mineralization. Lithos 89:424–446. https://doi.org/10.1016/j.lithos.2005.12.010

Webster JD, Duffield WA (1994) Extreme halogen abundances in tin-rich magma of the Taylor Creek Rhyolite, New Mexico. Econ Geol 89: 840–850. https://doi.org/10.2113/gsecongeo.89.4.840

Whalen JB, Currie KL, Chappell BW (1987) A-type granites: geochemical characteristics, discrimination and petrogenesis. Contrib Mineral Petrol 95:407–419. https://doi.org/10.1007/BF00402202

White AJR, Collins WJ, Chappell B (1982) Influence of melt structure on the trace element composition of granites. In: Proceedings of the International Symposium. Nanjing University, China, pp 737–751

Wilkinson JJ (2001) Fluid inclusions in hydrothermal ore deposits. Lithos 55:229–272. https://doi.org/10.1016/S0024-4937(00)00047-5

Wones DR (1989) Significance of the assemblage titanite+ magnetite+ quartz in granitic rocks. Am Mineral 74:744–749

Yang XM (2017) Estimation of crystallization pressure of granite intrusions. Lithos 286–287:324–329. https://doi.org/10.1016/j.lithos.2017.06.018

Zhao KD, Jiang SY, Dong CY, Chen WF, Chen PR, Ling HF, Zhang J, Wang KX (2011) Uranium-bearing and barren granites from the Taoshan Complex, Jiangxi Province, South China: Geochemical and petrogenetic discrimination and exploration significance. J Geochem Explor 110:126–135. https://doi.org/10.1016/j.gexplo.2011.04.006